Journal of Environmental Chemical Engineering 11 (2023) 110554

Contents lists available at ScienceDirect

Journal of Environmental Chemical Engineering

journal homepage: www.elsevier.com/locate/jece

Carbon nitride exfoliation for photocatalysis and photocatalytic ozonation over emerging contaminants abatement

Eryk Fernandes [a], Pawel Mazierski [b], Magdalena Miodyńska [b], Tomasz Klimczuk [c], Mirosława Pawlyta [d], Adriana Zaleska-Medynska [b], Rui C. Martins [a,*], João Gomes [a]

[a] University of Coimbra, CIEPQPF – Chemical Engineering Processes and Forest Products Research Center, Department of Chemical Engineering, Faculty of Sciences and Technology, Rua Sílvio Lima, Polo II, 3030-790 Coimbra, Portugal
[b] Faculty of Chemistry, Department of Environmental Technology, University of Gdansk, Wita Stwosza 63, 80-308 Gdańsk, Poland
[c] Department of Solid State Physics, Faculty of Applied Physics and Mathematics, Gdansk University of Technology, 80-233 Gdańsk, Poland
[d] Materials Research Laboratory, Faculty of Mechanical Engineering, Silesian University of Technology, Konarskiego 18A, 44-100 Gliwice, Poland

ARTICLE INFO

Editor: Despo Kassinos

Keywords:
g-C_3N_4
Catalysts exfoliation
Parabens
Photocatalytic oxidation
Photocatalytic ozonation

ABSTRACT

The production of graphitic carbon nitride was studied with the addition of a following exfoliation step using ultrasounds, at different times. The treatment produced catalysts with much higher surface areas, from 2.18 m^2 g^{-1} with no treatment to 28.34 m^2 g^{-1} after 36 h of exfoliation. During exfoliation, melem was also produced, and may further enhance the photoluminescence and photocatalytic properties. The photocatalytic reaction also indicated the improved performance of exfoliated g-C_3N_4 towards the degradation of a mixture of parabens, enhancing their removal from 20% to up to 65% in 2 h under UVA radiation. The combination of ozone and g-C_3N_4 photocatalysis was able to completely remove the parabens in under 8 min and with a 20% lower consumption of ozone compared to photolytic ozonation. The main reactive species were identified, and the by-products formed during parabens degradation were detected. The efficiency of the combined system was also attested by using a mixture of parabens and other common drugs, maintaining its better performance.

1. Introduction

Pharmaceuticals and personal care products (PPCPs) represent a highly valuable global market, accounting for numerous daily used goods and billions of euros annually [1]. This group encompasses different molecules, some categorized as contaminants of emerging concern (CECs), which are a group of pollutants that have increasingly been detected in multiple locations, lacking legislation and monitorization, and presenting at least a suspected negative effect on human and environmental health [2]. Parabens are examples of such contaminants, broadly applied as preservatives in PPCPs, in order to extend their shelf life, but also categorized as endocrine disruptive chemicals (EDCs) [3].

Another difficulty involving CECs is their elimination, as they typically present refractory characteristics and typical technologies present in water treatment facilities are not able to fully eliminate them [4]. Photocatalysis and other advanced oxidation processes (AOPs) are taken as excellent alternatives for the treatment of such pollutants, as they are based on the production of oxidative radicals, principally $^{\bullet}OH$, highly efficient and non-selective [5]. These processes can be further combined, for example in photocatalytic ozonation, to boost the overall efficiency and take advantage of both a great oxidant, such as ozone, and a faster production of radicals as a result of catalyst photoactivation [6].

In photocatalytic water treatment, TiO_2 is the most common material applied, due to its low-cost and optimized characteristics. Nonetheless, this semiconductor still presents some typical disadvantages, namely its high recombination rate of the photogenerated species and low absorption in the visible region [7]. In front of this, other alternative catalysts have been explored to obtain a more feasible material, capable of being activated through visible or solar radiation.

Graphitic carbon nitride (g-C_3N_4) is one of these visible-light-driven (VLD) materials, currently being the aim of various studies, possessing an interesting metal-free polymeric structure, good stability, and easy production [8,9]. Fernandes et. al [10] compared benchmark TiO_2 to a g-C_3N_4 catalyst produced through simple thermal polymerization of dicyandiamide, and regarding methyl-, ethyl- and propylparaben degradation using LED lamps, the polymeric catalyst eliminated the contaminants in 20 min, 6 times less than the compared material.

Still, g-C_3N_4 normally presents low specific surface areas and high

* Corresponding author.
E-mail address: martins@eq.uc.pt (R.C. Martins).

https://doi.org/10.1016/j.jece.2023.110554
Received 2 May 2023; Received in revised form 7 July 2023; Accepted 9 July 2023
Available online 12 July 2023

Table 1
Sample label, BET surface area, band gap values, position of conduction band (CB) and valance band (VB).

Sample label	Exfoliation time (h)	BET surface area (m^2 g^{-1})	Band gap value (eV)	An edge of a CB (eV)	An edge of a VB (eV)
CN	0	2.18	2.60	1.00	3.60
6CN	6	9.25	2.70	0.95	3.65
12CN	12	12.29	2.71	0.95	3.66
18CN	18	15.67	2.73	0.94	3.67
36CN	36	28.34	2.75	0.93	3.88

recombination rates of electron and positive holes, which can compromise the photoactivity of the catalyst. Thus, different techniques have been applied to suppress these disadvantages, such as the exfoliation of g-C_3N_4. The exfoliation can be conducted through different methods, thermal, chemical, or solvent ultrasonic-assisted, and can largely increase the material surface area, number of active sites, adsorptive performance, and dispersibility [11]. Lin et al. [12] used a mixture of ethanol, isopropanol, dimethyl formamide, and water as solvents in an ultrasonic-assisted treatment of g-C_3N_4 for 10 h. The treated catalyst presented more than 5 times higher BET surface area, 59.4 m^2 g^{-1}, lower electron and hole recombination rate, and complete elimination of RhB within 70 min against nearly 40% degradation of bulk g-C_3N_4 at the same time.

The use of g-C_3N_4 in photocatalytic ozonation has not been vastly explored, but some studies appointed its promising results. Orge et al. [13] obtained a full elimination of oxamic acid using a thermally treated g-C_3N_4 catalyst in the presence of ozone, with proved synergetic effect between the two used technologies. In our previous studies, bulk g-C_3N_4 was successfully used in the photocatalytic ozonation of parabens, despite drawbacks regarding its surface and photochemical properties [14].

Herein, the exfoliation of g-C_3N_4 using an alcohol solvent under ultrasound was successfully studied, with the treatment time being also evaluated from 6 h to 36 h of exposure. The catalyst was applied in a series of reactions for the degradation of parabens. The enhancement of the addition of ozone during photocatalysis and its interaction with the treated catalyst was also assessed. Multiple parameters and mechanisms were studied, to evaluate photoactivity in more complex water matrices, the main oxidative species involved in contaminants elimination, and the by-products formed in these reactions.

2. Materials and methods

2.1. Chemicals and Preparation of bulk and exfoliated g-C_3N_4

The methylparaben (MP), ethylparaben (EP), and propylparaben (PP) were obtained from Sigma-Aldrich. Isopropanol (IPA) (Sigma-Aldrich), 1,4-benzoquinone (BQ) (Sigma-Aldrich), and potassium iodide (KI) (Fluka) were used as radical scavengers. The main by-products standards, hydroquinone, 4-hydroxybenzoic acid (4-HB), 2,4-dihydroxybenzoic acid (2,4-DHB), and 3,4-dihydroxybenzoic acid (3,4-DHB) were obtained from Sigma-Aldrich, phenol from PanReac and acrylic acid from Acros.

For the synthesis of bulk g-C_3N_4, melamine (99%, Sigma-Aldrich) and methanol (analytical grade, STANLAB) were used applied. The preparation followed a typical thermal polymerization method [14]. Briefly, melamine was placed in covered ceramic crucibles and put in a furnace, for 4 h at 550 °C (2 °C min^{-1}). After the polymerization, the materials were self-cooled until room temperature, grounded, washed with methanol, and dried for 12 h at 60 °C.

The bulk g-C_3N_4 (CN) was then subjected to an exfoliation step, with different treatment times (6 – 36 h). In this step, the bulk g-C_3N_4 (CN) were introduced in bottles containing methanol, which were then placed in an ultrasonic bath (800 W, 50 Hz) for the respective times. Finally, the exfoliated g-C_3N_4 were obtained, 6CN, 12CN, 18CN, and 36CN, according to their treatment times as presented in Table 1.

2.2. Characterization techniques

The morphology of the bulk and exfoliated g-C_3N_4 catalysts was examined using a field-emission scanning electron microscope (FE-SEM/TEM; JEOL JSM-7610 F). To understand the crystal structure, a technique called powder X-ray diffraction was employed at room temperature using a Bruker D8 Focus diffractometer. This technique utilized Cu Kα radiation and a LynxEye XE-T detector, and the data was collected over a 30-minute scan time from $2\theta = 10–40°$. The diffuse reflectance spectra of the catalysts were measured using a UV-Vis spectrophotometer (UV 2600, Shimadzu) equipped with an integrating sphere in the range of 300–800 nm using a $BaSO_4$ as a reference. The specific surface area of the catalysts was determined by using the Brunauer–Emmett–Teller (BET) method, which measured the relative pressure range (p/p_0) 0.05–0.3 using a Micro 200 (3 P Instruments). Band gap as well as VB and CB calculations were made based on our previous report [15]. Fourier-transform infrared spectroscopy (FT-IR) analysis were performed in a FT-IR 4200 spectrometer (Jasco), with the tests been carried at room temperature. The sample's spectra were recorded with resolution of 4 cm^{-1}.

2.3. Experimental procedures

For each reaction, a 2 L solution containing a mixture of methylparaben (MP), ethylparaben (EP), and propylparaben (PP) was prepared, at a concentration of 1 mg L^{-1}. Additionally, during the mechanistic studies, to increase the complexity of the water matrix, other contaminants were introduced to the solution, namely paracetamol (PCT), carbamazepine (CBZ), and sulfamethoxazole (SMX), at 1 mg L^{-1} each. To identify the main oxidative species participating in the photocatalytic reactions, separately, 20 mM of isopropanol, 20 mM of potassium iodide, and 0.02 mM of 1,4-benzoquinone were used as radical scavengers [16]. Samples were taken at certain times, the catalysts were separated using 0.45 μm filters, and further analysis and contaminants quantification were conducted.

A jacked glass reactor (2 L) was used for all reactions, kept under continuous magnetic stirring and at 25 °C. In the photo-assisted reactions, 3 Philips TL 6 W BLB (16 mm) UVA lamps (λ_{mp}=365 nm) were employed. Ozone was produced, when applied, from a pure oxygen stream using an ozone generator (802 N, BMT), and inlet and outlet gas analyzers were respectively employed for the ozone detection in each stream. A potassium iodide (KI) solution was also used to trap the remaining ozone present in the outlet gas stream. To quantify the ozone that contributes to the contaminants' degradation reactions, the transferred ozone dose (TOD) was calculated following Eq. 1:

$$TOD = \int_0^t \frac{Q_G}{V_L} \times \left([O_3]_i - [O_3]_o\right) \quad dt \tag{1}$$

Where Q_G is the ozone inflow, 0.2 L min^{-1}, V_L the volume of liquid being treated, 2 L, and $[O_3]_i$ and $[O_3]_o$ the ozone concentration, mg L^{-1}, in the inlet and outlet reactor streams.

2.4. Analytical techniques

To identify and quantify contaminants concentration, a high-performance liquid chromatography (HPLC) (Waters 2695) was used, equipped with a C18 SiliChrom column, kept at 40 °C. The sample volume established was 100 μL, and the mobile phase was a 50/50 mixture of methanol and 0.1% orthophosphoric acid solutions, with a flow of 1 mL min^{-1}.

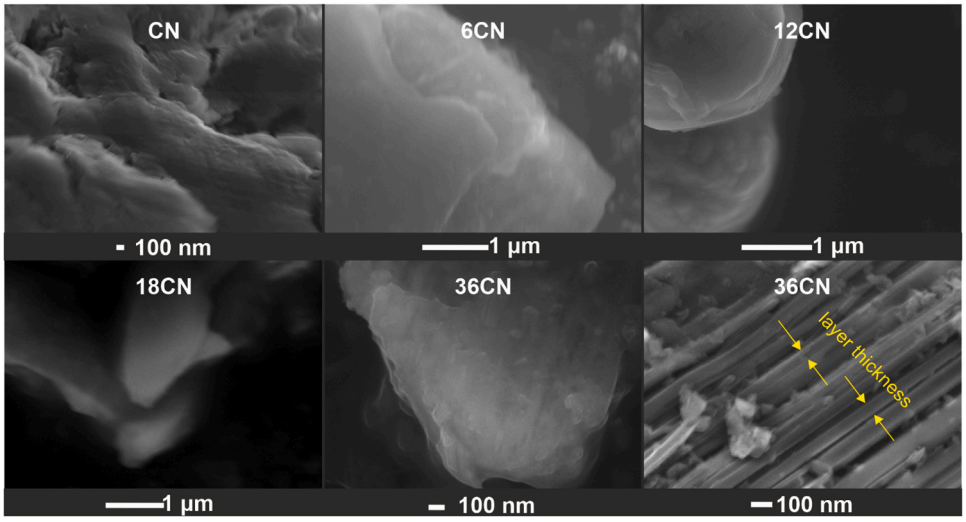

Fig. 1. Surface morphology (SEM images) of bulk and ultrasonically exfoliated g-C_3N_4 catalysts.

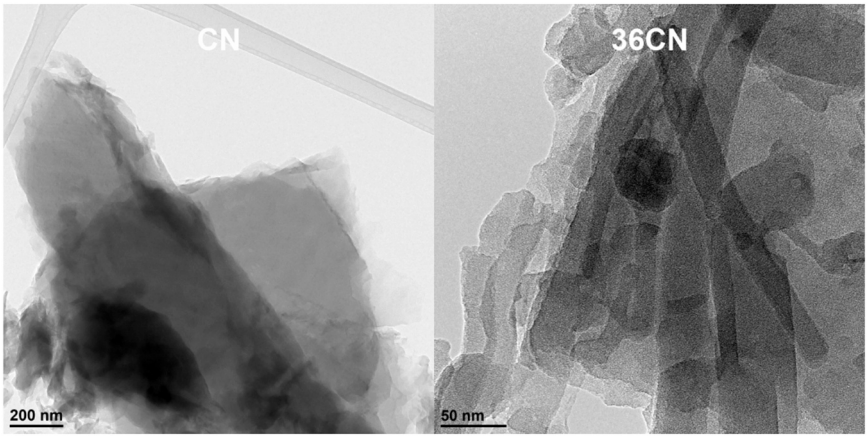

Fig. 2. TEM images of bulk and exfoliated g-C_3N_4 catalyst.

3. Results and discussion

3.1. *g-C_3N_4 characterization*

The surface morphology of the prepared bulk and exfoliated g-C_3N_4 catalysts is shown in Fig. 1. One can observe that the bulk C_3N_4 sample exhibited a highly compacted layered nature, which is in agreement with previous studies [14]. The treatment of this material with ultrasound resulted in the opening of its layered structure. With an increase in the duration of ultrasound treatment, it is possible to observe loosely packed individual layers of C_3N_4, which is particularly evident for the sample subjected to 36 h of ultrasound treatment. It can be also observed that the layers become thinner as the duration of the process increases, reaching a thickness of 45 ± 1.5 nm after 36 h of ultrasonic treatment. The observations from SEM images were confirmed by the TEM analysis (Fig. 2). Based on the presented TEM images, it is evident that the bulk C_3N_4 material undergoes the process of exfoliation, resulting in smaller layers.

The observations from SEM and TEM images were confirmed by the BET surface area analysis. The reference sample had a BET surface area of only 2.18 $m^2\ g^{-1}$, whereas, with the increase in ultrasonic treatment duration, the BET surface area increased (Table 1). The values of the BET surface area were 9.25, 12.29, 15.67, and 28.34 $m^2\ g^{-1}$ after 6, 12, 18, and 36 h of ultrasonic treatment, respectively. The C_3N_4 layers have become separated and smaller, which increases their BET surface area. Similar conclusions were drawn by Papailias et al. [17] who subjected melamine-derived C_3N_4 to chemical and thermal exfoliation. In this case, the C_3N_4 structure also opened up and the obtained C_3N_4 layers were characterized by a several-fold higher BET surface area.

Fig. 3a shows the results obtained from the investigation of the samples' optical properties using UV–vis diffuse reflectance spectroscopy measured in the range of 200 – 800 nm. The bulk C_3N_4 sample exhibited typical photoabsorption for a C_3N_4 material obtained by thermal polycondensation, with the absorption band extending up to 500 nm [18]. As can be seen, subjecting bulk C_3N_4 to ultrasonic treatment caused a blue shift in the optical absorption up to 450 nm which can be attributed to the quantum confinement effect due to the smaller size and thickness of the layers [19,20]. The observed changes in the photoabsorption properties of exfoliated C_3N_4 affected the band gap values, as shown in Fig. 3b. The band gap values obtained for all samples are presented in Table 1. Among the ultrasonically treated C_3N_4 samples, the band gap values differed slightly within the range of 2.7–2.75 eV. The larger band gap of the exfoliated catalysts may be attributed to the increased quantum size effect, and may also improve the separation of photogenerated species [21–23].

The positions of the conduction band (CB) and valence band (VB) in both the bulk and exfoliated g-C_3N_4 catalysts were calculated using [15], and the results are summarized in Table 1 and shown in Fig. 4(a comparison between the bulk and the most active exfoliated sample). It is evident that the CB and VB positions of the exfoliated catalysts have

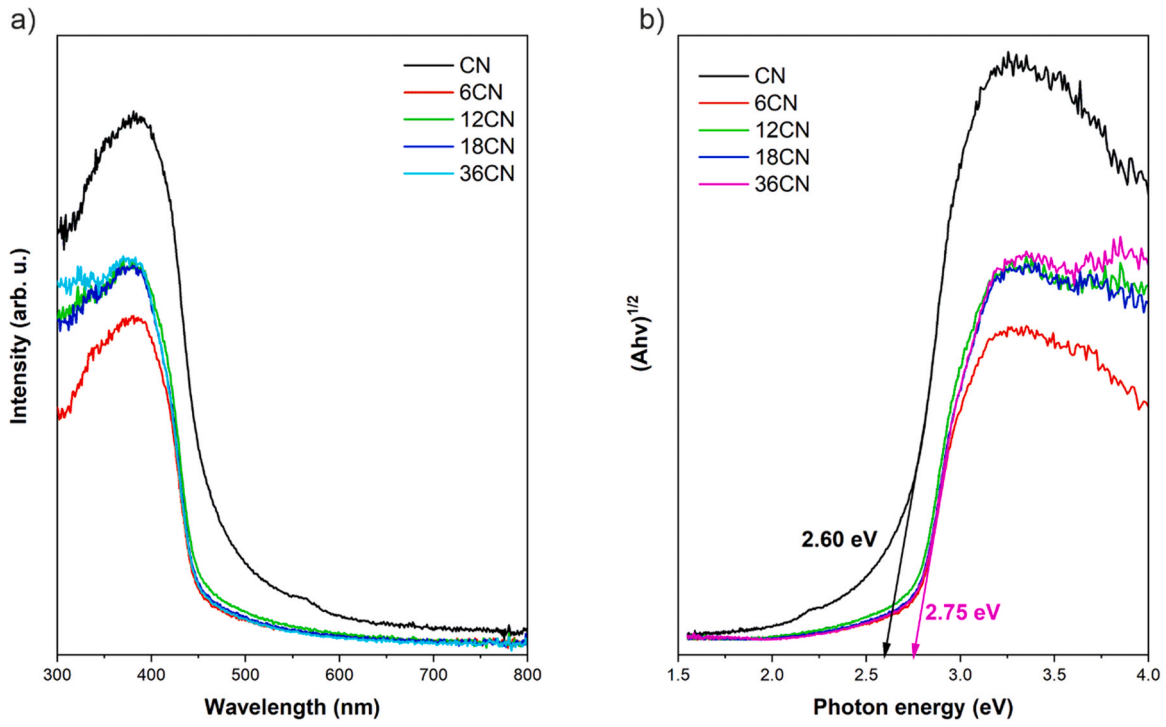

Fig. 3. a) Photoabsorption properties, and b) Tauc's plot of bulk and ultrasonically exfoliated g-C_3N_4 catalysts.

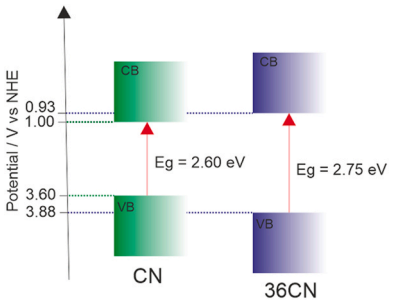

Fig. 4. Scheme of electronic band structures in bulk (CN) and exfoliated g-C_3N_4 catalysts (36CN).

shifted compared to the bulk sample, particularly in the case of the longest treated sample (36CN). This shift in band positions signifies several significant changes. Firstly, it can lead to the generation of a higher number of photoexcited electrons, resulting in a more efficient charge separation process [17,24,25]. Furthermore, the observation of a more positive VB value in the exfoliated g-C_3N_4 samples suggests improved mobility of the generated holes. This increased mobility, combined with the positive VB shift, enhances the photooxidation efficacy of the catalyst [24,25].

Fig. 5 shows the XRD patterns of both bulk and ultrasonically exfoliated g-C_3N_4. The bulk sample exhibits two characteristic peaks of g-C_3N_4 (marked in Fig. 5). One is a weak peak at 13.1° corresponding to the (100) plane, which is related to the in-plane structural packing of tri-s-triazine units [26,27]. The other is a strong diffraction peak at 27.2° corresponding to the (002) plane, which is attributed to the interlayer stacking of aromatic rings [28]. In the case of exfoliated g-C_3N_4 catalysts, the intensity of both (100) and (002) peaks decreased with the increasing time of ultrasonic treatment. This decreased intensity of the (100) and (002) peaks in comparison to bulk C_3N_4 can be attributed to a smaller planar size and a lower number of aligned layers, respectively [17]. Moreover, for sample 36CN, the (100) plane seems to be absent,

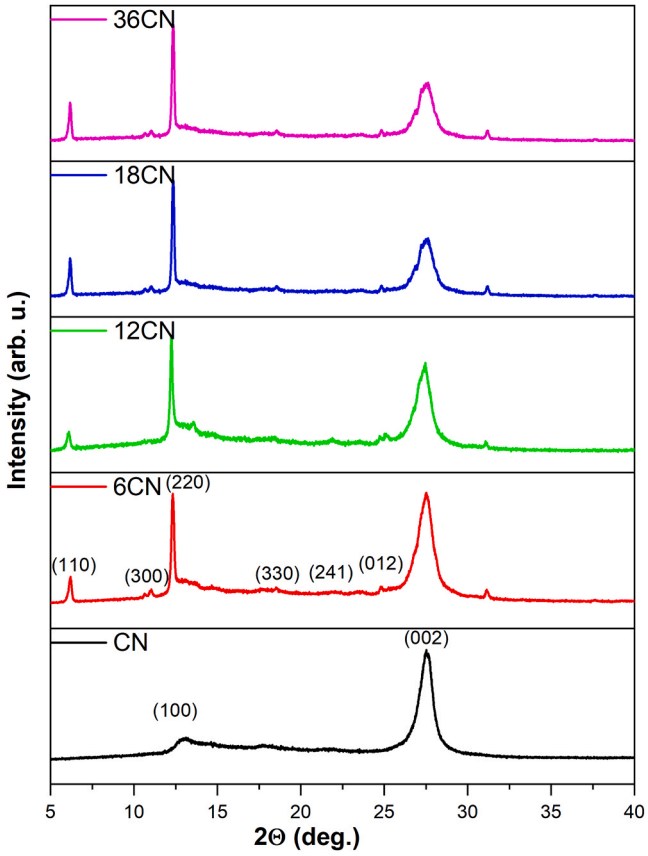

Fig. 5. pXRD patterns of bulk and exfoliated g-C_3N_4 catalysts.

indicating a significant reduction in the size of the layers as was observed in SEM images. In the diffraction patterns of exfoliated C_3N_4, there are also some new reflections (as marked in Fig. 3) that can be

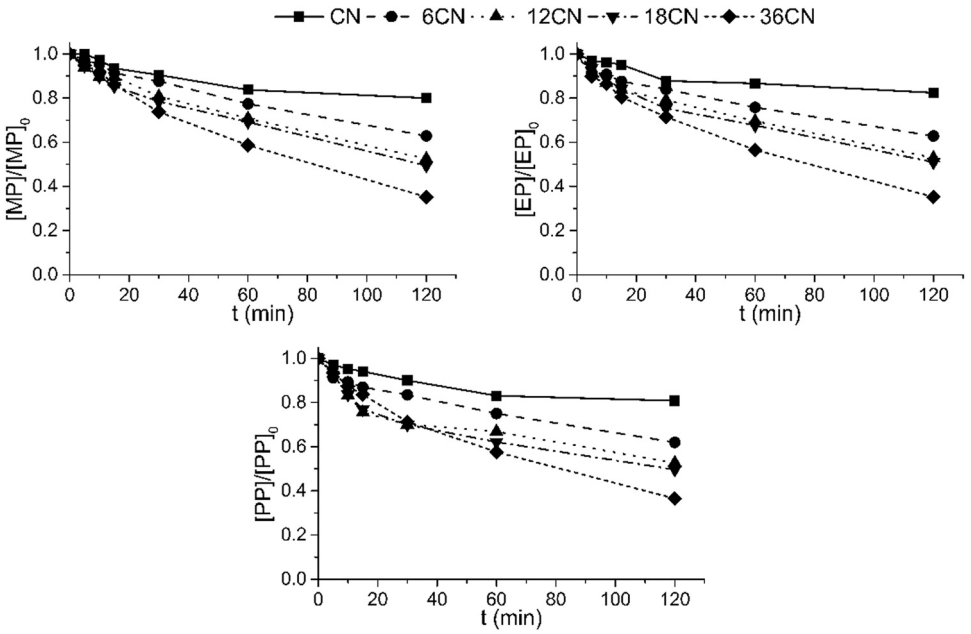

Fig. 6. Photocatalytic oxidation tests under UVA radiation for the degradation of 1 mg L^{-1} of a methyl-, ethyl- and propylparaben mixture, using bulk (CN) and exfoliated (6CN, 12CN, 18CN, and 36CN) g-C_3N_4.

attributed to melem [29,30]. g-C_3N_4 is a material formed by combining melem molecules, and its fundamental unit is composed of heptazine rings [31]. Nikookar et al. [32] demonstrated that the treatment of g-C_3N_4 obtained via thermal polycondensation of melamine with concentrated H_2SO_4 (95–98%) at 80 °C for a limited time resulted in the selective production of the monomer melem. Thus, subjecting the bulk C_3N_4 to ultrasonic treatment is likely to result in a similar effect (other than exfoliation and layer extraction), namely the disruption of the C-NH-C groups that connect the s-heptazine units, causing the release of individual triamino-s-heptazine molecules as monomers.

3.2. Photocatalytic oxidation

The bulk and exfoliated g-C_3N_4 catalysts were evaluated in photocatalysis reactions for the degradation of a parabens mixture (MP, EP, and PP) under ultraviolet-A radiation (Fig. 6). Ultraviolet radiation was selected in these initial tests as the radiation source as it was previously found that bulk g-C_3N_4 possessed low activity under visible radiation. The catalyst load used in this test was 200 mg L^{-1}, for the degradation of 1 mg L^{-1} of each contaminant. Prior to the photocatalytic reactions, the adsorption of parabens onto the catalysts' surface was investigated in the absence of light, and no significant alterations in the parabens' concentration were found after 24 h. Nonetheless, before every reaction, the catalyst was mixed with the solutions in the dark for 15 min to

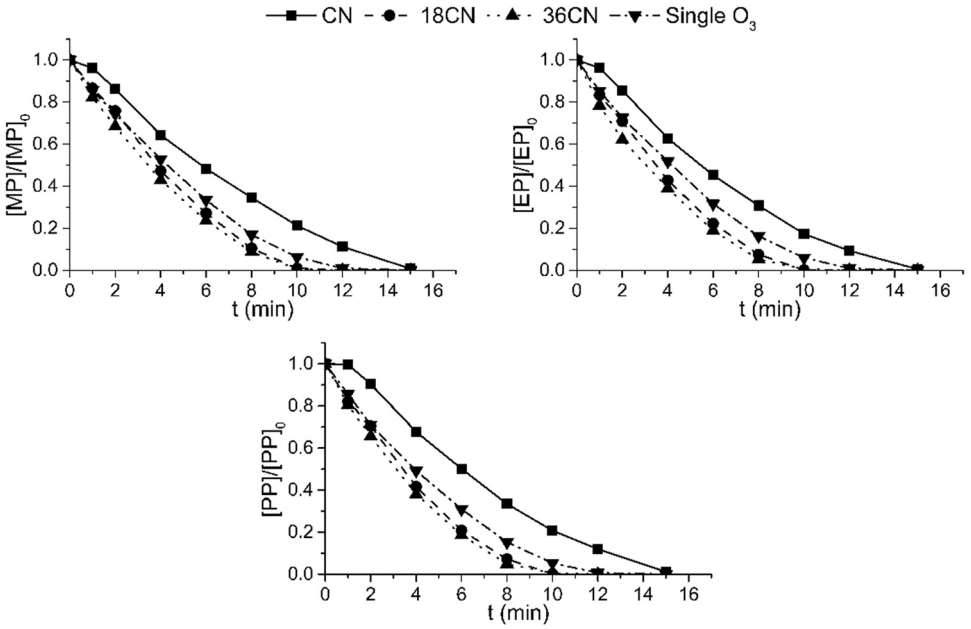

Fig. 7. Catalytic and single ozonation tests for the degradation of 1 mg L^{-1} of a methyl-, ethyl- and propylparaben mixture, using bulk (CN) and exfoliated (18CN and 36CN) g-C_3N_4.

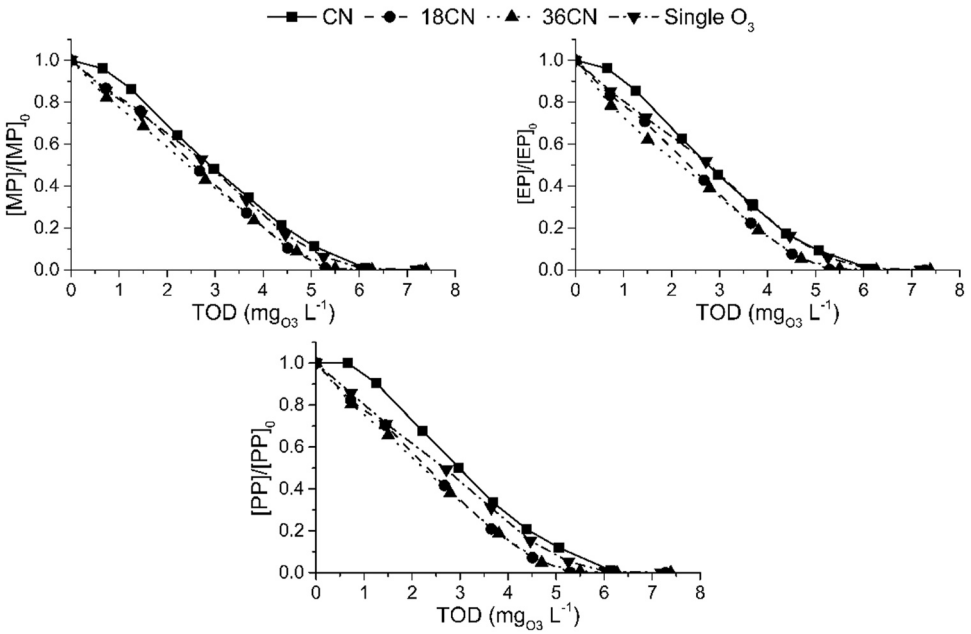

Fig. 8. Catalytic and single ozonation tests for the degradation of 1 mg L^{-1} of a methyl-, ethyl- and propylparaben mixture over the respective transferred ozone doses (TOD), using bulk (CN) and exfoliated (18CN and 36CN) g-C_3N_4.

guarantee a homogeneous dispersion and adsorption equilibrium. The elimination of each paraben was similar, with a slightly faster removal of regarding the longer-chain contaminants.

Upon the analysis of the contaminants' degradation evolution throughout time, it is evident an improvement in the catalyst performance with the exfoliation treatment. Compared to the bulk g-C_3N_4, methylparaben removal in 120 min increased from 20% to more than 37% with only 6 h of exfoliation. Regarding the increasing time of exfoliation, it was verified a parallel great improvement in the catalyst photoactivity, achieving up to 65% removals for the 36 h exfoliated catalyst.

The improved performance of the exfoliated catalyst is in agreement with their increased S_{BET} (Table 1). The exfoliation treatment is intended to dissociate the multiple stacked polymeric tri-s-triazine layers bounded by Van der Waals forces, leading into a more 2D sheet-like structure [33]. The obtained material possesses an improved specific surface, number of active sites, and electron mobility, resulting then in a higher interaction with the contaminants and the medium, increasing their elimination and radicals' production.

Another possible explanation for the improved photocatalytic performance is the appointed formation of melem during the exfoliation step. These molecules may promote a synergetic effect in combination with g-C_3N_4 and improve its properties, such as reduced recombination of photogenerated electron and hole pairs and further increase the material's surface area [29].

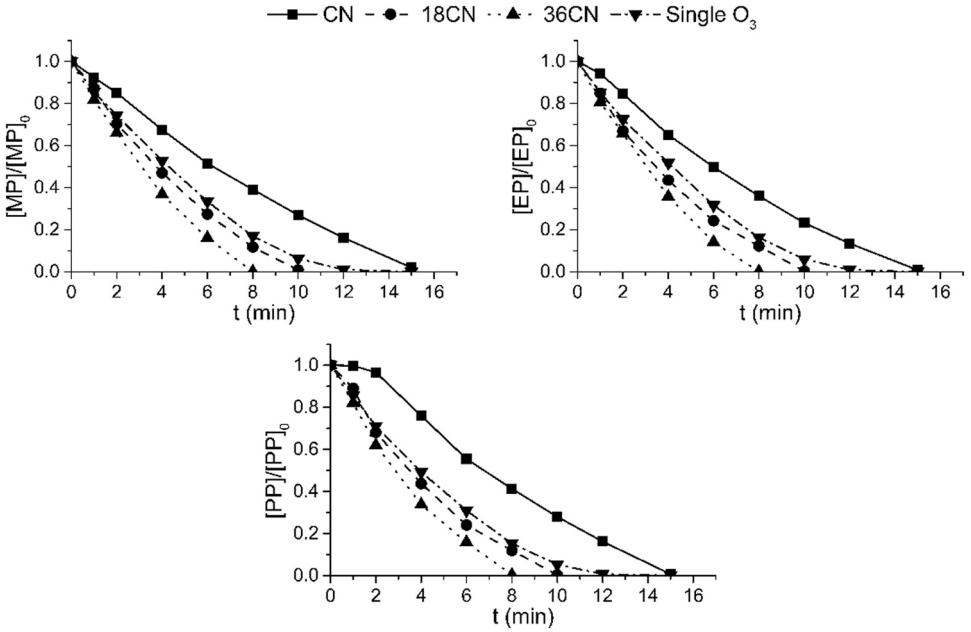

Fig. 9. Photocatalytic and single ozonation tests under UVA radiation for the degradation of 1 mg L^{-1} of a methyl-, ethyl- and propylparaben mixture, using bulk (CN) and exfoliated (18CN and 36CN) g-C_3N_4.

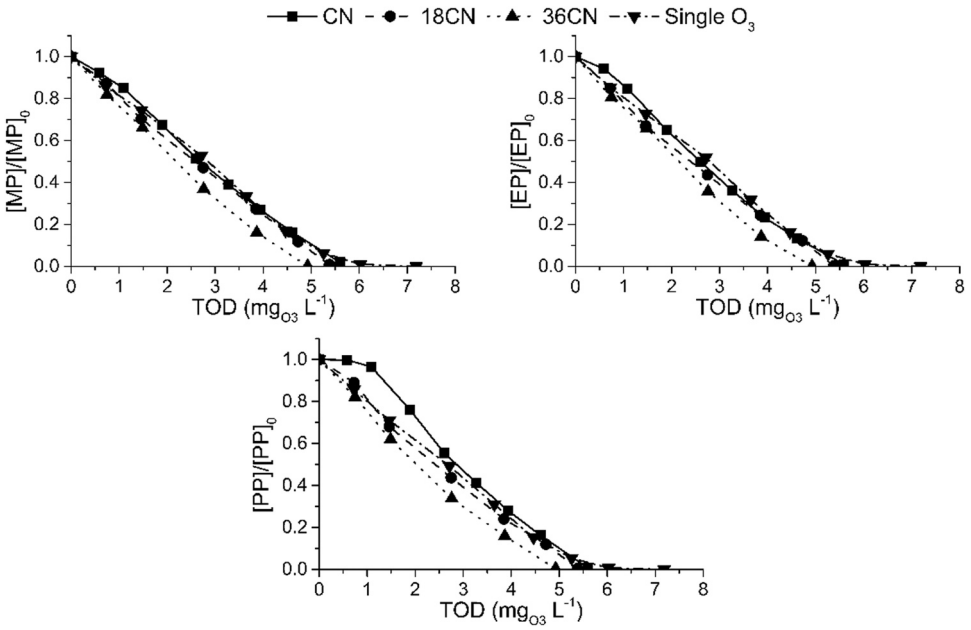

Fig. 10. Photocatalytic and single ozonation tests under UVA radiation for the degradation of 1 mg L^{-1} of a methyl-, ethyl- and propylparaben mixture over the respective transferred ozone doses (TOD), using bulk (CN) and exfoliated (18CN and 36CN) g-C_3N_4.

3.3. Catalytic and photocatalytic ozonation

To evaluate the effect of the addition of ozone in the reaction medium, catalytic and photocatalytic ozonation were performed with the two exfoliated catalysts with superior performances selected after the photocatalytic oxidation tests (18CN and 36CN), together with the bulk catalyst (CN). For comparative reasons, single ozonation reactions were also conducted and plotted alongside the catalytic-based tests (Fig. 7).

During the catalytic ozonation treatment of parabens, all reactions achieved complete removal of the contaminants, proving the high efficiency of ozone-based processes. In reference to the exfoliated catalysts, is clear the improvement in their photoactivity comparing both 36CN and 18CN to the bulk catalyst.

In fact, bulk g-C_3N_4 catalytic ozonation was found to be less efficient than single ozonation itself. Due to the electrophilic characteristics of ozone, it possesses a high affinity towards the aromatic rings present in the parabens' structure. This makes the direct reaction between molecular ozone and the contaminants a highly favored mechanism. In the gas-liquid-solid mixture of catalytic ozonation, part of the ozone present can be decomposed by the catalyst through the adsorption of the gas into the material surface, producing other radicals, such as hydroxyls ($^{\bullet}OH$), which would promote a faster degradation due to its elevated oxidative potential. In this scenario, the explanation for the lower performance of bulk g-C_3N_4 would be its low porosity and surface area, which entail higher mass transference resistances between the different phases, as described in previous studies [14,34]. Moreover, instead of efficiently promoting the production of highly oxidative radicals, ozone adsorption onto the catalyst surface may decrease its respective radical availability and vacant active sites of the catalyst, consequently resulting in a slower removal.

After the exfoliation treatment, the materials used in the catalytic systems provide a faster degradation of parabens than single ozonation, achieving a complete elimination in under 10 min. These results evidentiate the improvement in the physicochemical properties of the material, especially their porosity and specific surface areas, decreasing the mass transference resistances and facilitating radicals' production and a better harnessing of the ozone present in the medium.

Regarding ozone consumption, the transferred ozone doses (TOD) along the reactions were calculated (Fig. 8). For complete removal of contaminants, around 5.3 and 5.5 mg_{O3} L^{-1} was necessary using 18CN and 36CN catalyst, which is slightly more than a 9% decrease in comparison to single ozonation, 6.0 mg_{O3} L^{-1}. Even if it also corroborates the improvement towards ozone decomposition due to the exfoliation treatment, a slight difference between the ozone consumption is expected in the absence of light and the catalyst photoactivation.

In the photocatalytic ozonation (Fig. 9) reactions are possible to attest to a more noticeable difference regarding the time of exfoliation treatment. While bulk CN and 18CN maintained a similar behavior as in the catalytic tests, a considerable improvement was found for the 36 h exfoliated g-C_3N_4, completely removing all contaminants in under 8 min

The exfoliation treatment, aside from the physicochemical alterations, may also promote an enhancement of the photoelectric characteristics of the catalyst. After photon irradiation, the excited e^- and positive holes are separated and lead to the formation of numerous radicals, through interaction with the molecules present in the medium (e.g., H_2O, O_2, O_3), and by the direct attack to the contaminants after their adsorption on the surface of the material. The separation of such photogenerated species, which possess a tendency to easily recombine, and the mobility of the electrons are key aspects of the photocatalytic process and are known drawbacks in the case of g-C_3N_4 [29]. Thus, the exfoliation of g-C_3N_4 may break the C-NH-C groups connecting the s-heptazine units, and alter surface properties, band potentials, and photon absorption characteristics that can overcome these drawbacks [33].

The consumption of ozone was also reduced using 36CN in the presence of UVA radiation (Fig. 10). Compared to the catalytic ozonation, the photocatalytic reaction presented a reduction of the necessary TOD from 5.5 to 4.9 mg_{O3} L^{-1}, around 20% less than single ozonation. The decrease in the ozone dose needed to achieve full elimination of contaminants is a result of a boosted utilization and decomposition of ozone by g-C_3N_4, and poses an important economic advantage, as the overall process cost is greatly associated with energy consumption for ozone production.

3.4. Detection of main reactive species

To better understand the mechanisms in the photocatalytic oxidation reactions using 36CN, three different radical scavengers were added in

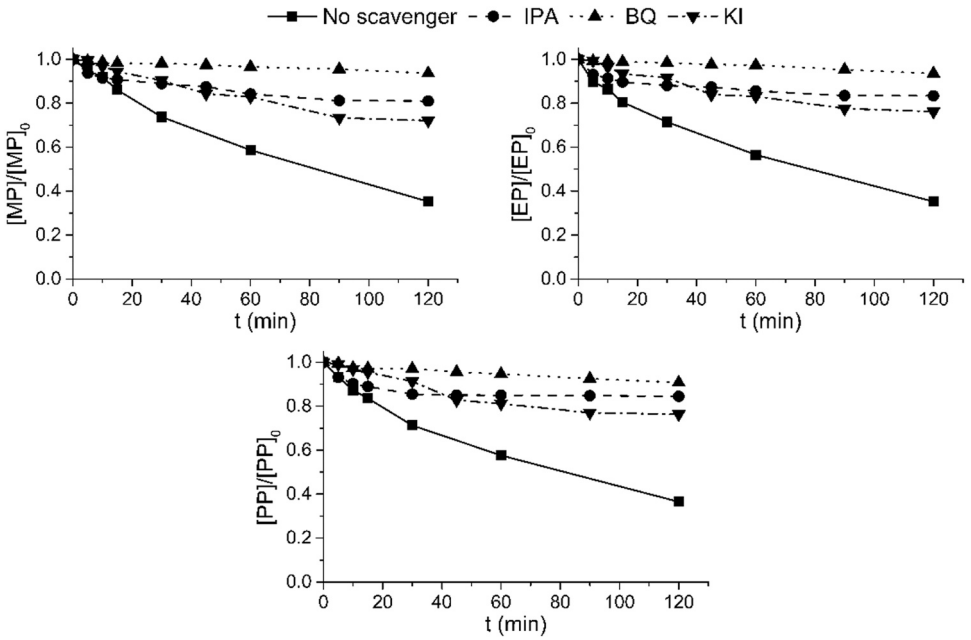

Fig. 11. Photocatalytic oxidation using 36CN in the presence of 20 mM of isopropanol (IPA), 0.02 of 1,4-benzoquinone (BQ), and 20 mM of potassium iodide (KI), separately.

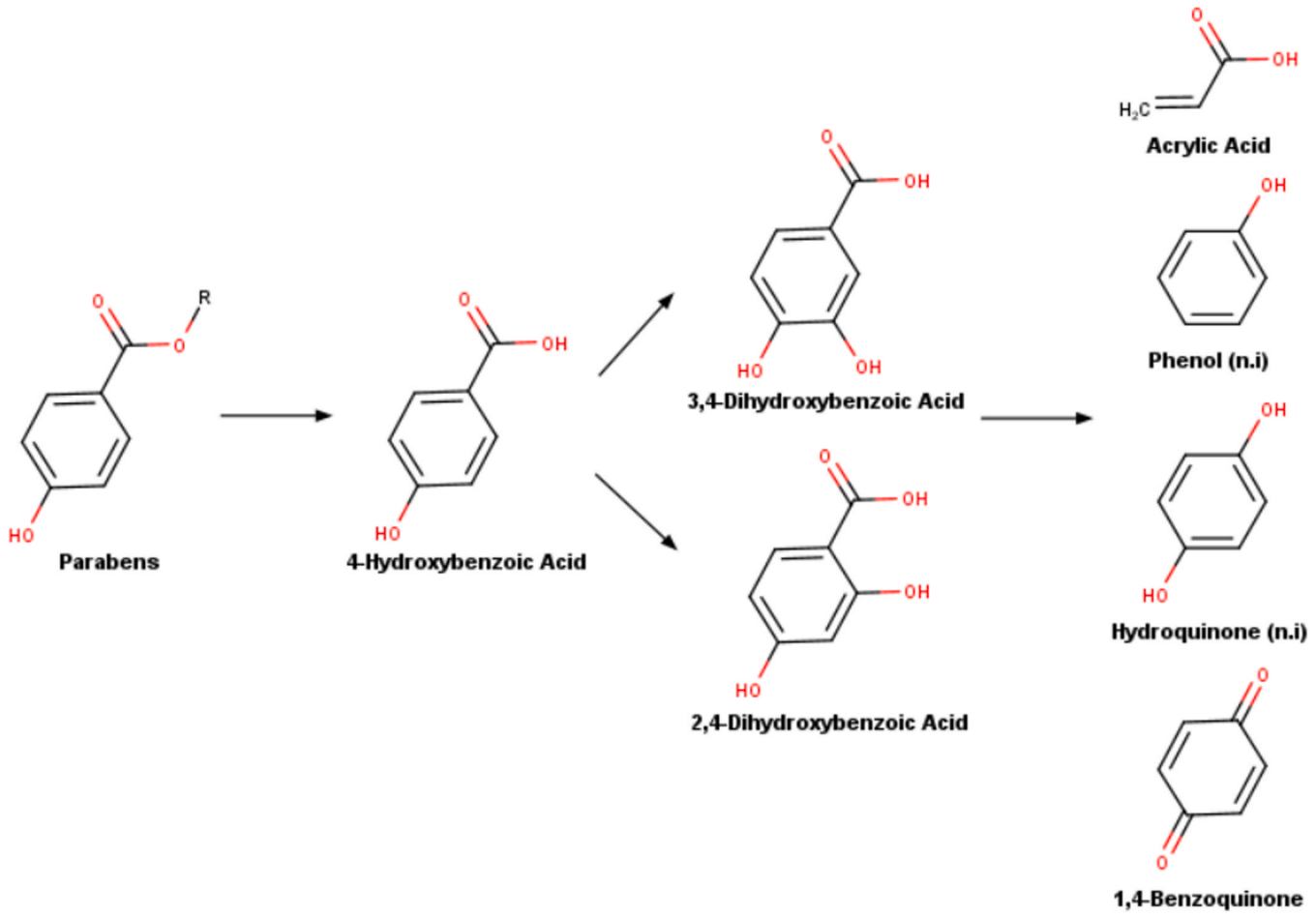

Fig. 12. Possible degradation paths and by-products formed during the photocatalytic degradation of parabens.

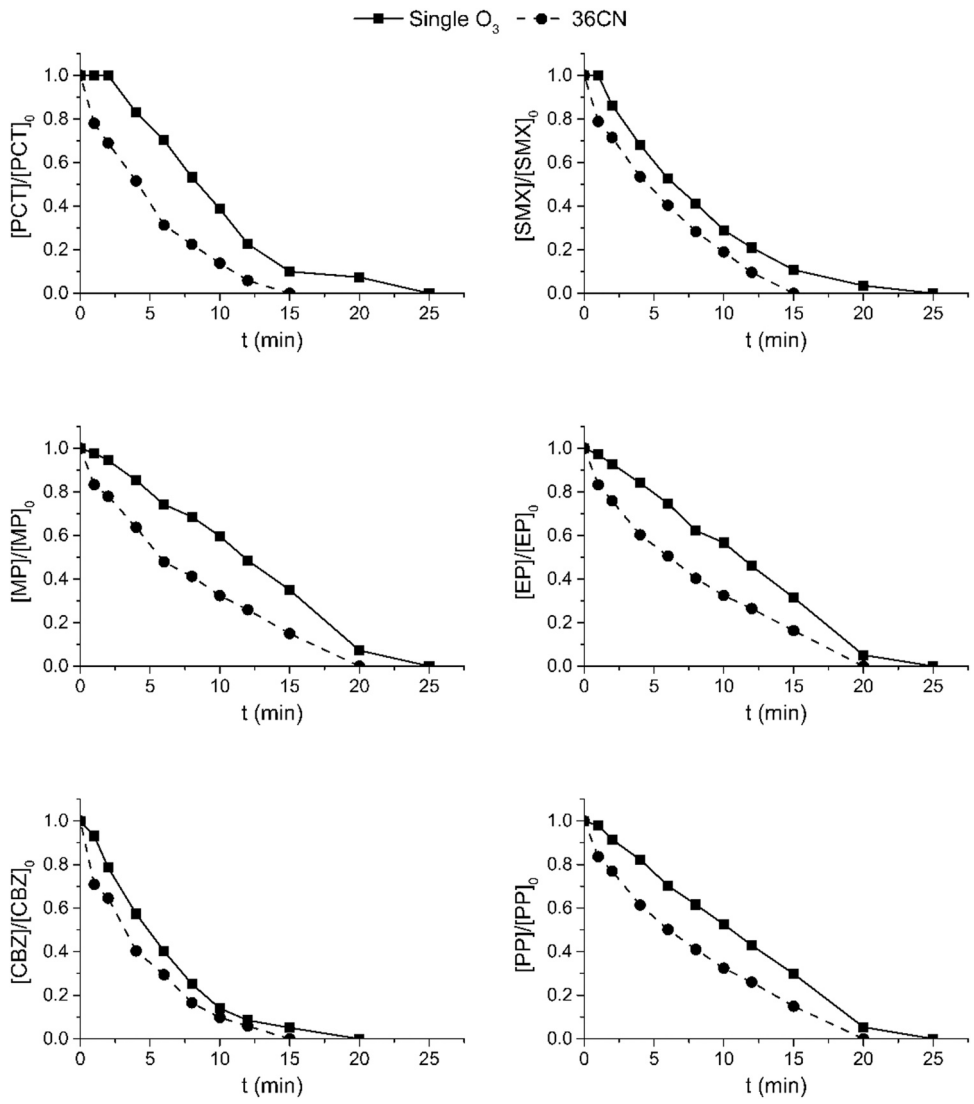

Fig. 13. Photocatalytic (36CN) and single ozonation tests under UVA radiation for the degradation of 1 mg L^{-1} of a paracetamol (PCT), sulfamethoxazole (SMX), methylparaben (MP), ethylparaben (EP), carbamazepine (CBZ) and propylparaben (PP) mixture.

different tests, isopropanol (IPA), 1,4-benzoquinone (BQ), and potassium iodide (KI), as $^{\bullet}OH$, $^{\bullet}O_2^-$ and h^+ scavengers, respectively (Fig. 11). The use of any of the three scavengers greatly affected the removal of parabens, indicating that all three radicals evaluated possess important and concomitant roles in the photocatalytic reactions. The use of KI as an h^+ scavenger, even at a lower degree compared to the other scavenger, considerably decreased the parabens removal, from 65% to 28%. Similarly, to KI, IPA addition reduced to 19% the degradation of parabens, as expected due to the higher efficiency of hydroxyl radicals. Lastly, $^{\bullet}O_2^-$ proved to be a crucial radical in the photocatalytic elimination of parabens, with only 0.02 mM of BQ drastically reducing their removal to around 7%, which was also found in other studies involving g-C_3N_4 catalysts [13,35]. The highlighted role of $^{\bullet}O_2^-$, as an efficient electron receptor, can be a possible explanation for the prevalence of by-products formed through oxidation, such as 1,4-benzoquinone compared to hydroquinone.

3.5. By-products identification

Using the exfoliated g-C_3N_4 catalyst with the best results, 36CN, an analysis of the possible by-product formation was made. The degradation of parabens led to the formation of mainly 5 different species, which were detected in different stages of the reaction. In the four reaction configurations, photocatalytic oxidation, photocatalytic ozonation, catalytic ozonation, and photolytic ozonation, the same species were detected, only different regarding their concentration.

The possible route of degradation is present in Fig. 12. The 4-hydroxybenzoic acid (4-HB) was detected in the first moments of all reactions and has been appointed to be a predominant species directly formed from parabens degradation [36,37]. 4-HB is formed by the dealkylation and hydroxylation of parabens, caused by the attack of hydroxyl radicals to the terminal carbon of the methyl, ethyl, and propyl chains. The 3, 4-dihydroxybenzoic and 2,4-dihydroxybenzoic acids were also detected and are formed by the consequent hydroxylation of the benzenic ring. This further hydroxylation is considerably fast, as 4-HB was first detected at 5 min of photocatalytic oxidation, with its maximum concentration at 10 min, when the concentration of other hydroxybenzoic acids starts to increase. This transformation occurs even faster in the presence of ozone, as 2,4-DHB and 3,4-DHB were already detected in the first 2 min of the reactions. Hydroquinone (HQ) is also commonly found in parabens by-products', formed through dealkylation and decarboxylation, and may be further photo-oxidized into 1,4-benzoquinone (BQ) [38]. In the sample tested, HQ was not detected, indicating that it is rapidly oxidized into BQ, as it starts to appear in the first minutes of the reactions. Phenol is another possible aromatic by-product that is commonly found, occurring due to the decarboxylation of 4-HB, but it

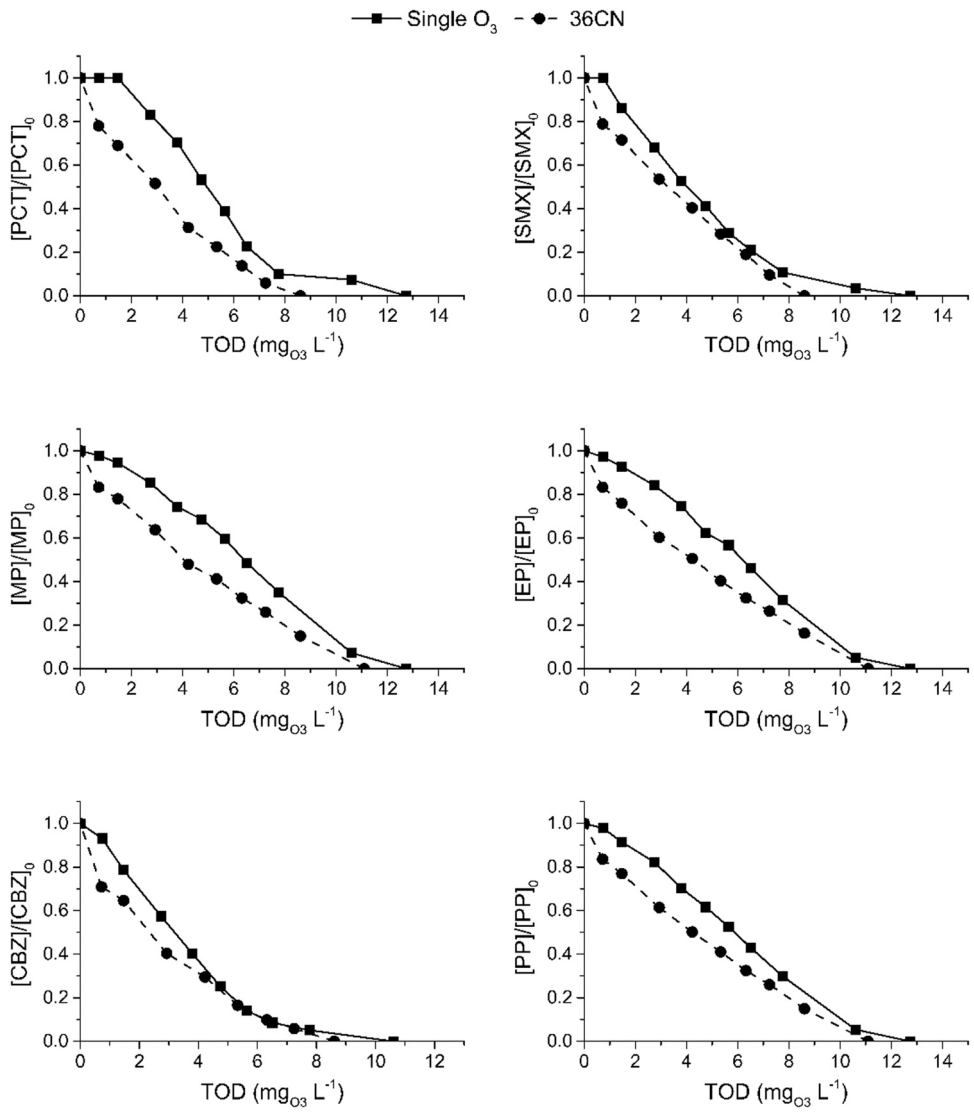

Fig. 14. Photocatalytic (36CN) and single ozonation tests under UVA radiation for the degradation of 1 mg L^{-1} of paracetamol (PCT), sulfamethoxazole (SMX), methylparaben (MP), ethylparaben (EP), carbamazepine (CBZ) and propylparaben (PP) mixture over the respective transferred ozone doses (TOD).

was not detected, possibly existing in concentrations lower than the detection limit [37,39].

After the formation of more simple aromatic molecules, ring-opening transformations occurs, forming other open-chain compounds, such as maleic and xylonic acids [40]. These compounds are further oxidized into shorter-chain molecules, mostly carboxylic acids such as acrylic acid, which was detected in the analyzed samples, leading to their mineralization, forming CO_2 and H_2O.

3.6. Water matrix complexity

As ozone and parabens possess a high affinity, the processes of single ozonation by itself present already an efficient removal rate. Thus, even though already significantly improving the overall efficiency of such contaminant mixture removal, photocatalytic ozonation is expected to enhance even more the performance compared to the separated technologies for more complex solutions. In more realistic scenarios, multiple contaminants and other parameters will influence the treatment reaction, so the chosen technology must present a more non-selective and still efficient performance.

To evaluate the behavior of the selected catalyst (36CN) in more complex water, three contaminants were added to the solution alongside the parabens, which were Sulfamethoxazole (SMX), Carbamazepine (CBZ), and Paracetamol (PCT) (Fig. 13). These three substances were selected as they are highly and daily used drugs, which are prone to reach the wastewater treatment plants, that do not possess the necessary technologies to fully eliminate them, posing a danger to human and environmental health.

In this mixture of contaminants is possible to better visualize the significance of the catalyst in this treatment system. A complete treatment of the pollutants present in the mixture was obtained at 20 min for 36CN photocatalytic ozonation and 25 min for single ozonation. Carbamazepine possessed similar degradation profiles for both photocatalytic and single ozonation, probably due to its higher number of aromatic structures. Nonetheless, to fully remove this drug from the medium, it was necessary 15 min for the catalytic reaction in comparison to 20 min of ozonation. In the case of the treatment of pharmaceuticals, is especially important to achieve their complete elimination, as small remnant amounts may lead to the formation of resistant strains of microorganisms and still may possess chronic health effects.

The parabens, as was appointed previously, already have a higher affinity towards ozone attack. However, in this medium is possible to verify in the plotted data a faster decrease in the concentrations throughout time. This occurrence is intrinsically connected to higher

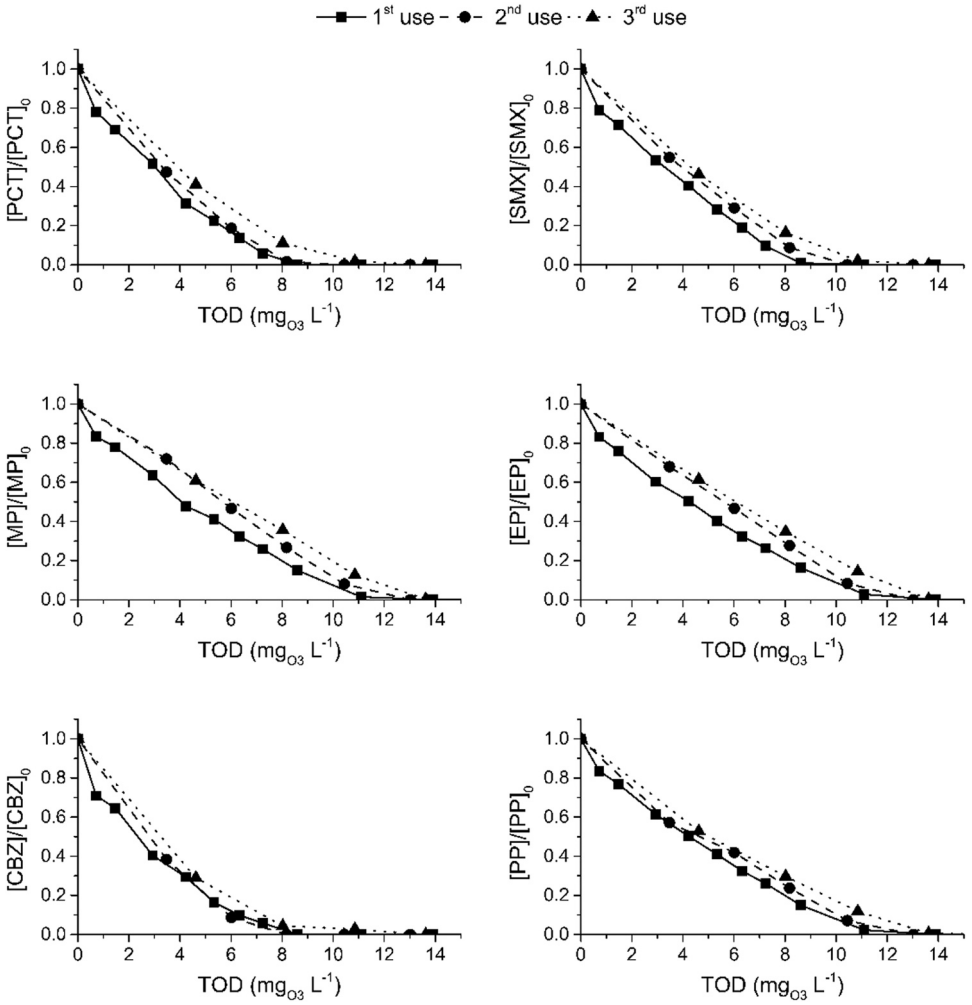

Fig. 15. Photocatalytic ozonation using reused 36CN under UVA radiation for the degradation of 1 mg L^{-1} of paracetamol (PCT), sulfamethoxazole (SMX), methylparaben (MP), ethylparaben (EP), carbamazepine (CBZ) and propylparaben (PP) mixture over the respective transferred ozone doses (TOD).

kinetics and reaction rates.

Paracetamol and sulfamethoxazole presented the more distinct profiles, requiring 15 min of the photocatalytic treatment against 25 min in the absence of the studied material. These pharmaceuticals present sulfur and nitrogen groups, and less electron-rich sites, reducing their susceptibility to ozone attack.

The consumption of ozone was also reduced in the presence of the catalyst, with a decrease of around 20% to completely remove all contaminants, similar to the parabens mixture results (Fig. 14).

3.7. Catalyst reuse

In order to evaluate the capacity of reutilization of the exfoliated g-C_3N_4 catalyst, three consecutive uses of the material were performed, being applied in reactions for the degradation of the mixture of 6 contaminants in combination with ozone (Fig. 15). After each reaction, the catalyst was filtered, dried, and then used in the following reaction. The volume of the solution was adapted according to the amount of catalyst recovered, to maintain the same catalyst load (200 mg L^{-1}) in all

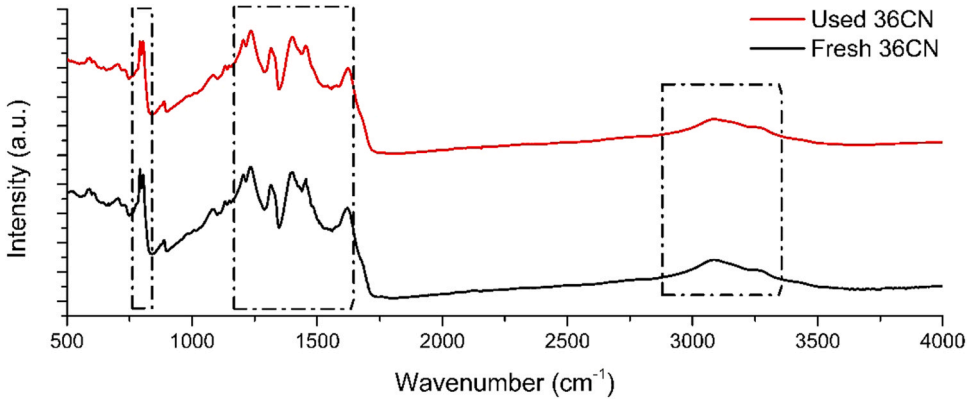

Fig. 16. FT-IR spectra of fresh and used 36CN.

reactions, as some material is lost during the material separation.

After the three uses of the catalyst, some difference in the transferred ozone dose can be observed, although not in a high amount. Regarding the degradation of the contaminants along time, no significant variations were found, maintaining a similar elimination as presented previously. This alteration regarding ozone may be caused by the variations in the volume of the reaction to maintain the catalyst concentration. As a low density and thin powder catalyst, the recuperation of the exfoliated g-C_3N_4 is a known challenge for its application in larger scales, which is commonly made through filtration, presenting a considerable amount of material lost.

Nonetheless, other possible explanations for the small decrease in efficiency may be the blockage of active sites by the contaminants and even the deactivation caused by ozone, which can alter the material structure, promoting the formation or breakage of chemical bounds, for example introducing oxygen in catalyst structure [13]. To evaluate the latter, Fourier-transform infrared spectroscopy (FT-IR) analysis were conducted to both fresh and used samples of the catalyst (Fig. 16).

In the FT-IR spectra of g-C_3N_4, three regions are particularly distinct. The first peak, around 800 cm^{-1}, corresponds to the breathing mode of the triazine units. The second region, 1250–1650 cm^{-1} containing multiples peaks is referent to different stretching modes heterocyclic C-N bounds. Finally, the broad peak around 3100 cm^{-1} is correspondent of the stretching of N-H in the -NH_2 functional groups [8,9,15,17]. Moreover, no changes in the spectra of both samples can be noted, indicating that the intrinsic structure of material is preserved after multiple uses.

4. Conclusions

The thermal polymerization synthesis of g-C_3N_4 catalysts was successfully conducted. Exfoliation treatment of the produced catalysts was proved to greatly improve the physicochemical properties of the materials, as well as their photoactivity, as indicated by their characterization. The production of melem through the rupture of C-NH-C groups connecting the s-heptazine units during exfoliation may also improve the catalyst properties.

A degradation of 65% of the mixture of parabens was obtained using a 36 h exfoliated g-C_3N_4, an improvement from only 20% of the bulk material within 2 h. This higher efficiency is a result of a higher surface area obtained after the physical treatment, increasing the interaction between the catalyst and the medium, conjointly with a possible decrease of photocarrier recombination.

The $^{\bullet}OH$, $^{\bullet}O_2^-$ and h^+ radicals presented significant and simultaneous roles in the photocatalytic reactions, especially $^{\bullet}O_2^-$, as the reaction was drastically impeded in its absence. The main by-products formed in the photocatalytic degradation of parabens were identified and an overall route was appointed.

The combination of photocatalysis and ozonation was able to remove the pollutants from the mixture in under 8 min, with a decrease of 20% of the consumed ozone, compared to single photolytic ozonation. Moreover, applied for the treatment of a mixture containing 6 different pollutants, once again requiring a lower reaction time and ozone consumption, proving its efficacy in more complex water matrices. Moreover, the reuse of the catalyst indicated that the overall structure of the material is maintained, and the efficacy of the treatment is high even after consecutive uses.

These obtained results demonstrate the versatility and efficiency of the use of g-C_3N_4 in photocatalytic ozonation as a feasible water treatment technology, in addition to the benefits of a simple exfoliation method able to improve the material properties.

Funding

This work was supported by the European Structural and Investment Funds through Portugal2020 by the project Photo-SupCatal—Development of supported catalytic systems for wastewater treatment by photo-assisted processes (POCI-01-0247-FEDER-047545). The authors gratefully acknowledge FCT (Fundação para a Ciência e Tecnologia, Portugal) for the PhD Grant (2020.06130.BD) and the financial support (CEECIND/01207/2018). Thanks are due to FCT/MCTES for the financial support to CIEPQPF (UIDB/00102/2020).

CRediT authorship contribution statement

Eryk Fernandes: Writing – original draft, Conceptualization, Investigation, Visualization, Methodology, Funding acquisition. **Pawel Mazierski:** Resources, Writing – review & editing, Visualization, Methodology, Funding acquisition. **Magdalena Miodyńska:** Resources, Writing – review & editing, Visualization, Methodology, Funding acquisition. **Tomasz Klimczuk:** Resources, Visualization, Methodology, Funding acquisition. **Mirosława Pawlyta:** Resources, Visualization, Methodology. **Adriana Zaleska-Medynska:** Resources, Writing – review & editing, Visualization, Methodology, Funding acquisition. **João Gomes:** Methodology, Resources, Conceptualization, Writing – review & editing, Visualization, Supervision, Funding acquisition. **Rui C. Martins:** Methodology, Resources, Conceptualization, Writing – review & editing, Visualization, Supervision, Funding acquisition.

Declaration of Competing Interest

The authors declare that they have no known competing financial interests or personal relationships that could have appeared to influence the work reported in this paper.

Data Availability

Data will be made available on request.

References

[1] K. Nowak, E. Jabłońska, W. Ratajczak-Wrona, Controversy around parabens: alternative strategies for preservative use in cosmetics and personal care products, Environ. Res. 198 (2021), https://doi.org/10.1016/j.envres.2020.110488.
[2] J.W. Lee, H.K. Lee, H.B. Moon, Contamination and spatial distribution of parabens, their metabolites and antimicrobials in sediment from Korean coastal waters, Ecotoxicol. Environ. Saf. 180 (2019) 185–191, https://doi.org/10.1016/j.ecoenv.2019.05.012.
[3] G.M.B. Louis, M.M. Smarr, L. Sun, Z. Chen, M. Honda, W. Wang, R. Karthikraj, J. Weck, K. Kannan, Endocrine disrupting chemicals in seminal plasma and couple fecundity, Environ. Res. 163 (2018) 64–70, https://doi.org/10.1016/j.envres.2018.01.028.
[4] M.C.V.M. Starling, C.C. Amorim, M.M.D. Leão, Occurrence, control and fate of contaminants of emerging concern in environmental compartments in Brazil, J. Hazard. Mater. 372 (2019) 17–36, https://doi.org/10.1016/j.jhazmat.2018.04.043.
[5] H. Sun, F. Guo, J. Pan, W. Huang, K. Wang, W. Shi, One-pot thermal polymerization route to prepare N-deficient modified g-C_3N_4 for the degradation of tetracycline by the synergistic effect of photocatalysis and persulfate-based advanced oxidation process, Chem. Eng. J. 406 (2021), 126844, https://doi.org/10.1016/j.cej.2020.126844.
[6] E. Fernandes, S. Contreras, F. Medina, R.C. Martins, J. Gomes, N-doped titanium dioxide for mixture of parabens degradation based on ozone action and toxicity evaluation: precursor of nitrogen and titanium effect, Process Saf. Environ. Prot. (2020), https://doi.org/10.1016/j.psep.2020.03.006.
[7] J.A. Khan, M. Sayed, S. Khan, N.S. Shah, D.D. Dionysiou, G. Boczkaj, Advanced oxidation processes for the treatment of contaminants of emerging concern, in: Contam. Emerg. Concern Water Wastewater Adv. Treat. Process., Elsevier Inc, 2019, pp. 299–365, https://doi.org/10.1016/B978-0-12-813561-7.00009-2.
[8] G. Dong, Y. Wen, H. Fan, C. Wang, Z. Cheng, M. Zhang, J. Ma, S. Zhang, Graphitic carbon nitride with thermally-induced nitrogen defects: an efficient process to enhance photocatalytic H_2 production performance, RSC Adv. 10 (2020) 18632–18638, https://doi.org/10.1039/d0ra01425g.
[9] X. Chang, H. Fan, L. Lei, X. Wu, W. Wang, L. Ma, Generation mechanism of the defects in g-C_3N_4 synthesized in N_2 atmosphere and the method for improving photocatalysis activity, Catalysts 13 (2023), https://doi.org/10.3390/catal13020269.
[10] R.A. Fernandes, M.J. Sampaio, G. Dražić, J.L. Faria, C.G. Silva, Efficient removal of parabens from real water matrices by a metal-free carbon nitride photocatalyst, Sci. Total Environ. 716 (2020), https://doi.org/10.1016/j.scitotenv.2019.135346.
[11] M. Zhang, Y. Yang, X. An, J. Zhao, Y. Bao, L. an Hou, Exfoliation method matters: the microstructure-dependent photoactivity of g-C_3N_4 nanosheets for water

purification, J. Hazard. Mater. 424 (2022), 127424, https://doi.org/10.1016/j.jhazmat.2021.127424.
[12] Q. Lin, L. Li, S. Liang, M. Liu, J. Bi, L. Wu, Efficient synthesis of monolayer carbon nitride 2D nanosheet with tunable concentration and enhanced visible-light photocatalytic activities, Appl. Catal. B Environ. 163 (2015) 135–142, https://doi.org/10.1016/j.apcatb.2014.07.053.
[13] C.A. Orge, M.J. Sampaio, J.L. Faria, M.F.R. Pereira, C.G. Silva, Efficiency and stability of metal-free carbon nitride in the photocatalytic ozonation of oxamic acid under visible light, J. Environ. Chem. Eng. 8 (2020), 104172, https://doi.org/10.1016/j.jece.2020.104172.
[14] E. Fernandes, S. Drosopoulou, P. Mazierski, M. Miodynska, D. Gołaszewska, A. Zaleska-Medynska, R.C. Martins, J. Gomes, Carbon nitride photoactivation evaluation and degradation of a mixture of parabens by ozone assistance, J. Water Process Eng. 49 (2022), https://doi.org/10.1016/j.jwpe.2022.103018.
[15] L.S.G. Velázquez, M.L. Dell'Arciprete, L. Madriz, M.C. Gonzalez, Carbon nitride from urea: Mechanistic study on photocatalytic hydrogen peroxide production for methyl orange removal, 175 (2023). https://doi.org/10.1016/j.catcom.2023.106617.
[16] I. Papailias, N. Todorova, T. Giannakopoulou, N. Ioannidis, N. Boukos, C. P. Athanasekou, D. Dimotikali, C. Trapalis, Chemical vs thermal exfoliation of g-C_3N_4 for NOx removal under visible light irradiation, Appl. Catal. B Environ. 239 (2018) 16–26, https://doi.org/10.1016/j.apcatb.2018.07.078.
[17] G. Xin, Y. Meng, Pyrolysis synthesized g-C_3N_4 for photocatalytic degradation of methylene blue, J. Chem. 2013 (2013), https://doi.org/10.1155/2013/187912.
[18] X. Yuan, C. Zhou, Y. Jin, Q. Jing, Y. Yang, X. Shen, Q. Tang, Y. Mu, A.K. Du, Facile synthesis of 3D porous thermally exfoliated g-C_3N_4 nanosheet with enhanced photocatalytic degradation of organic dye, J. Colloid Interface Sci. 468 (2016) 211–219, https://doi.org/10.1016/j.jcis.2016.01.048.
[19] J. Tong, L. Zhang, F. Li, K. Wang, L. Han, S. Cao, Rapid and high-yield production of g-C_3N_4 nanosheets via chemical exfoliation for photocatalytic H_2 evolution, RSC Adv. 5 (2015) 88149–88153, https://doi.org/10.1039/c5ra16988g.
[20] W. Wang, J. Fang, H. Chen, Nano-confined g-C_3N_4 in mesoporous SiO_2 with improved quantum size effect and tunable structure for photocatalytic tetracycline antibiotic degradation, J. Alloy. Compd. 819 (2020), 153064, https://doi.org/10.1016/j.jallcom.2019.153064.
[21] Y. Yin, J. Han, X. Zhang, Y. Zhang, J. Zhou, D. Muir, R. Sutarto, Z. Zhang, S. Liu, B. Song, Facile synthesis of few-layer-thick carbon nitride nanosheets by liquid ammonia-assisted lithiation method and their photocatalytic redox properties, RSC Adv. 4 (2014) 32690–32697, https://doi.org/10.1039/c4ra06036a.
[22] S. Yang, Y. Gong, J. Zhang, L. Zhan, L. Ma, Z. Fang, R. Vajtai, X. Wang, P. M. Ajayan, Exfoliated graphitic carbon nitride nanosheets as efficient catalysts for hydrogen evolution under visible light, Adv. Mater. 25 (2013) 2452–2456, https://doi.org/10.1002/adma.201204453.
[23] K. Maślana, R.J. Kaleńczuk, B. Zielińska, E. Mijowska, Synthesis and characterization of nitrogen-doped carbon nanotubes derived from g-C3N4, Materials 13 (2020), https://doi.org/10.3390/ma13061349.
[24] H. Yan, Y. Chen, S. Xu, Synthesis of graphitic carbon nitride by directly heating sulfuric acid treated melamine for enhanced photocatalytic H_2 production from water under visible light, Int. J. Hydrog. Energy 37 (2012) 125–133, https://doi.org/10.1016/j.ijhydene.2011.09.072.
[25] Y. Wang, W. Yang, X. Chen, J. Wang, Y. Zhu, Photocatalytic activity enhancement of core-shell structure g-C_3N_4@TiO_2 via controlled ultrathin g-C_3N_4 layer, Appl. Catal. B Environ. 220 (2018) 337–347, https://doi.org/10.1016/j.apcatb.2017.08.004.
[26] J. Mo, N. Wang, S. Zhang, X. Chen, J. Fu, P. Chen, Z. Liang, Q. Su, X. Li, Metal-free g-C_3N_4/melem nanorods hybrids for photocatalytic degradation of methyl orange, Res. Chem. Intermed. 48 (2022) 3835–3849, https://doi.org/10.1007/s11164-022-04779-6.
[27] T. Dai, H. Kiuchi, H. Minamide, Y. Miyake, H. Inoki, Y. Sonoda, J. Tsutsumi, K. Kanai, Growth and characterization of melem hydrate crystals with a hydrogen-bonded heptazine framework, Phys. Chem. Chem. Phys. 24 (2022) 13922–13934, https://doi.org/10.1039/d2cp00691j.
[28] M. Michalska, V. Matějka, J. Pavlovský, P. Praus, M. Ritz, J. Serenčíšová, L. Gembalová, M. Kormunda, K. Foniok, M. Reli, G. Simha Martynková, Effect of Ag modification on TiO_2 and melem/g-C_3N_4 composite on photocatalytic performances, Sci. Rep. 13 (2023) 1–20, https://doi.org/10.1038/s41598-023-32094-6.
[29] M. Nikookar, A. Rezaeifard, Maasoumeh Jafarpour, K.V. Grzhegorzhevskii, A. A. Ostroushko, A top-down design for easy gram scale synthesis of melem nano rectangular prisms with improved surface area, RSC Adv. 11 (2021) 38862–38867, https://doi.org/10.1039/d1ra07440g.
[30] S.P. Pattnaik, A. Behera, R. Acharya, K. Parida, Green exfoliation of graphitic carbon nitride towards decolourization of Congo-Red under solar irradiation, J. Environ. Chem. Eng. 7 (2019), 103456, https://doi.org/10.1016/j.jece.2019.103456.
[31] E. Fernandes, P. Mazierski, T. Klimczuk, A. Zaleska-medynska, R.C. Martins, g-C_3N_4 for photocatalytic degradation of parabens: precursors influence, the radiation source and simultaneous ozonation, Evaluation 13 (2023) 789, https://doi.org/https://doi.org/10.3390/ catal13050789.
[32] X. Jin, Y. Wu, Q. Zhang, F. Wang, P. Chen, H. Liu, S. Huang, J. Wu, N. Tu, W. Lv, G. Liu, Defect-modified reduced graphitic carbon nitride (RCN) enhanced oxidation performance for photocatalytic degradation of diclofenac, Chemosphere 258 (2020), 127343, https://doi.org/10.1016/j.chemosphere.2020.127343.
[33] A. Petala, R. Bontemps, A. Spartatouille, Z. Frontistis, M. Antonopoulou, I. Konstantinou, D.I. Kondarides, D. Mantzavinos, Solar light-induced degradation of ethyl paraben with CuO_x/$BiVO_4$: statistical evaluation of operating factors and transformation by-products, Catal. Today 280 (2017) 122–131, https://doi.org/10.1016/j.cattod.2016.04.045.
[34] A.G. Alhamzani, T.A. Yousef, M.M. Abou-Krisha, K.Y. Kumar, M.K. Prashanth, L. Parashuram, B. Hun Jeon, M.S. Raghu, Fabrication of layered In_2S_3/WS_2 heterostructure for enhanced and efficient photocatalytic CO_2 reduction and various paraben degradation in water, Chemosphere 322 (2023), 138235, https://doi.org/10.1016/j.chemosphere.2023.138235.
[35] M. Peñas-Garzón, M.J. Sampaio, Y.L. Wang, J. Bedia, J.J. Rodriguez, C. Belver, C. G. Silva, J.L. Faria, Solar photocatalytic degradation of parabens using UiO-66-NH_2, 286 (2022). https://doi.org/10.1016/j.seppur.2022.120467.
[36] J.F. Gomes, A. Lopes, M. Gmurek, R.M. Quinta-Ferreira, R.C. Martins, Study of the influence of the matrix characteristics over the photocatalytic ozonation of parabens using Ag-TiO_2, Sci. Total Environ. 646 (2019) 1468–1477, https://doi.org/10.1016/j.scitotenv.2018.07.430.
[37] X. Zhang, X. Wang, J. Meng, Y. Liu, M. Ren, Y. Guo, Y. Yang, Robust Z-scheme g-C_3N_4/WO_3 heterojunction photocatalysts with morphology control of WO_3 for efficient degradation of phenolic pollutants, Sep. Purif. Technol. 255 (2021), 117693, https://doi.org/10.1016/j.seppur.2020.117693.